

An approach to investigating the feasibility of free-space optical communication technology deployment under scintillation effects

Aras S. Mahmood

Physics Department, College of Education, University of Sulaimani, Sulaimani, Kurdistan Region / Iraq

Article info

Article history:

Received 26 Jun. 2023

Received in revised form 01 Aug. 2023

Accepted 04 Aug. 2023

Available on-line 30 Aug. 2023

Keywords:

Free-space optical communication;
atmospheric turbulence;
scintillation attenuation;
refractive index structure parameter
(C_n^2).

Abstract

Local weather conditions have an impact on the availability of free-space optical (FSO) communication. The variation in meteorological parameters, such as temperature, humidity, and wind speed, leads to variations of the refractive index along the transmission path. These refractive index inhomogeneities produced by atmospheric turbulence induce optical turbulence which is responsible for random fluctuations in the intensity of the laser beam that carries the signal (irradiance) called scintillations that can significantly degrade the performance of FSO systems. This paper aims to investigate the feasibility of deploying FSO communication technology under scintillation effects in any urban region and atmospheric environment. To achieve that, firstly by utilizing the Hufnagel-Vally day with the Sadot and Kopeika models together, the scintillation strength for a specified region, Sulaimani City in north-eastern Iraq as an example, has been estimated through the calculation of the refractive index structure parameter (C_n^2) over a period of 10 years and it was found to be at the strong turbulence level. Secondly, from the same estimated parameter, the scintillation attenuation of the signal carrying the laser beam intensity can be calculated to investigate the feasibility of FSO communication using Optysystem-7 software. The optimal link distance for north-eastern Iraq (Sulaimani City) has been found to be within the limit of about 5.5 km. Analysing the max. Q-factor, bit-error rate and signal to noise ratio for an average of 120 months between 2013–2022 assessed the best and worst seasons for FSO.

1. Introduction

Transmission of data between two points through light propagation in free space refers to free-space optical (FSO) communication which is an alternative to fibre optic communication. This kind of wireless optical communication technology uses a highly directed narrow light beam avoiding challenges faced by fibre optic communication such as high cost of digging roads, ease of installation, and high data rates. Immunity to interference, absence of radiation hazards, no need for licensed frequency band allocation, and, lastly, security are important issues in communication between two or more parties [1]. Among the three helpful wavelengths of FSO (850 nm, 1310 nm,

and 1550 nm), a 1550 nm wavelength is less attenuated and, also, has a good signal to noise ratio (SNR) as compared to the others [2]. It is more appropriate because it will not affect human eyes and its disadvantage is that it cannot be used if the attenuation is high for long distances [3]. FSO communication technique requires a clear line of sight between the transmitter and the receiver, so it is explicitly sensitive to bad weather conditions such as rain, snow, fog, dust, haze, aerosol, and turbulence. These conditions act to degrade the performance of the communication through light attenuation and could block the light path in the atmosphere. Rather than the attenuation due to molecular absorption that occurs when light propagates and hits the atmospheric atoms and the Mie or aerosol scattering, there is another effective attenuation due to scintillation phenomena [4, 5].

*Corresponding author at: aras.mahmood@univsul.edu.iq

2. Scintillation and atmospheric turbulence

The scintillation phenomenon refers to a random variation of strength of an optical signal as it propagates through atmospheric layers and will fluctuate and spread due to irregular changes in the transmission path over time [6, 7]. The reflection of solar power by the Earth's surface irregularly heats the atmosphere layers and produces different cells with different temperatures with the aid of wind velocity and different humidity, leading to atmospheric turbulence. This turbulence varies the refractive index or the optical characteristics of the medium layers, affecting the signal propagation and causing fluctuations in both its phase and amplitude, that is, it produces optical turbulence. The quantity that measures the strength of the optical turbulence is known as the refractive index structure parameter (C_n^2) [8]. Different authors give different values for weak to strong turbulence levels [6–12]. On average, it can be said that C_n^2 values are more than considered strong and less than considered weak turbulence. Rather than meteorological variables, C_n^2 depends on the geographical location, altitude (h), and time of day.

Reference 13 summaries almost all the models for predicting the evaluation of the C_n^2 . Of all of them, regarding the role of elevation above ground level (altitude h), the Hufnagel-Valley day model is the most appropriate for calculating the C_n^2 as a function of altitude, which is given by (1) below:

$$C_n^2(h) = 0.00594 \left(\frac{v}{27}\right)^2 \cdot (10^{-5}h)^{10} \cdot e^{(-h/1000)} + 2.7 \cdot 10^{-16} e^{(-h/1500)} + A e^{(-h/100)} \quad (1)$$

where A is the constant and equals $1.7 \cdot 10^{-14} \text{ m}^{-2/3}$ for $h = 0$, v is the wind speed in m/s, and h is the altitude in m. To get a precise value of C_n^2 , another model was used including the effect of the total cross-sectional area ($TCSA$) of aerosol particulates per m^3 and the solar flux (SF) was introduced by Sadot and Kopeika [7, 13] which is given as

$$C_n^2 = 5.9 \cdot 10^{-15} W_{th} + 1.6 \cdot 10^{-15} T - 3.7 \cdot 10^{-15} RH + 6.7 \cdot 10^{-17} RH^2 - 3.9 \cdot 10^{-19} RH^3 - 3.7 \cdot 10^{-15} WS + 1.3 \cdot 10^{-15} WS^2 - 8.2 \cdot 10^{-17} WS^3 + 2.8 \cdot 10^{-14} SF - 1.8 \cdot 10^{-14} TCSA + 1.4 \cdot 10^{-14} TCSA^2 - 3.9 \cdot 10^{-13} \quad (2)$$

where T is the temperature in K, RH is the relative humidity, SF is the solar flux and its value is 1.37 kW/m^2 , W_{th} is the temporal hour weight (0.1), WS is the speed of wind in m/s, and $TCSA$ in cm^2/m^3 gives the unit of C_n^2 in $\text{m}^{-2/3}$. The $TCSA$ is given by [7] as below:

$$TCSA = 7.3 \cdot 10^{-3} + 9.96 \cdot 10^{-4} RH - 2.75 \cdot 10^{-5} RH^2 - 1.37 \cdot 10^{-5} SF^4 \quad (3)$$

A precise measurement of the scintillation uses the total C_n^2 rather than only one of them [13], i.e.

$$C_n^2(\text{total}) = C_n^2 + C_n^2(h) \quad (4)$$

Rytov proposed that the refractive index variation of the atmospheric channel layers would alter the laser beam propagation, producing different patterns in time and space. The normalised Rytov variance, or the scintillation index (σ_1^2) is the parameter expressing these irradiance fluctuations. The fluctuations, $\sigma_1^2 > 1$ and $\sigma_1^2 < 1$ indicate strong and weak fluctuations regimes, respectively [7, 8].

Rytov expressed the scintillation index σ_1^2 as a function of the total C_n^2 as shown below:

$$\sigma_1^2 = K C_n^2 k^{7/6} L^{11/6} \cdot [\text{unitless}] \quad (5)$$

Here K is the constant equal to 0.5 for a spherical wave and 1.23 for a plane wave, k is the wave number and equals $\frac{2\pi}{\lambda}$ where λ is the beam wavelength in nm and L is the link distance in m [8]. The peak-to-peak amplitude of the scintillation equals $4\sigma_1$ and the scintillation attenuation equals $2\sigma_1$ [4], so the relation of the scintillation or turbulence attenuation denoted by α_{scint} in dB given by [8] for all turbulence levels, especially for spherical wave, is given below:

$$\alpha_{scint} = 2\sigma_1 = 2 \sqrt{\left(0.5 C_n^2 \left(\frac{2\pi}{\lambda}\right)^{7/6} L^{11/6}\right)} \quad (6)$$

In this work, the C_n^2 strength level has been estimated and used to analyse the impact of the scintillation on the FSO communication performance and its feasibility. The simulation analysis has been performed with the aid of Optisystem-7 software.

3. Methods and materials

For any specified region, the feasibility of FSO communication deployment can be analysed by estimating the scintillation strength using the combined Hufnagel-Vally (HV) day model and Sadot, Kopeika models together to include both the effects of optical turbulence, which has an important microphysical effect that produces significant intensity fluctuations, and basing entirely on macroscale meteorological parameters, respectively, for estimating C_n^2 . In this work, secondary dates of relative humidity (%), temperature ($^{\circ}\text{C}$), and wind speed (m/s) from the Sulaimani City meteorology station with a specified altitude were used as a study case. The monthly average of 120 months from 2013 to 2022 for the previous parameters is tabulated in Table 1.

3.1 Studied area

In this work, Sulaimani City located in north-eastern Iraq, at an altitude h of 884.8 m above sea level was selected for the study. Its longitude and latitude are 45.27 and 35.33, respectively, over an area of 20 144 km^2 , with a population of 779 000. Using Optisystem-7 software, the FSO communication link shown in Fig. 1 below has been proposed and tested to see the feasibility and performance of the link under scintillation effects.

Table 1.

Relative humidity, temperature, and wind speed average data for years from 2013 to 2022.

Month	Relative humidity (%)	Temperature (° C)	Wind speed (m/s)
January	70.04	7.22	1.1
February	65.69	9.37	1.27
March	61.74	12.97	1.45
April	54.35	18.22	1.21
May	42.47	24.27	1.37
June	29.01	30.37	1.52
July	26.02	34.02	1.65
August	26.57	33.99	1.51
September	31.25	29.26	1.25
October	44.55	22.57	1.29
November	61.43	14.41	1.1
December	69.35	9.63	0.89

3.2. Simulation design

Figure 1 shows the layout of a block diagram designed in OptiSystem-7 software. It mainly comprises three major parts: the transmission part contains a continuous-wave laser source operating at 1550 nm, which is safe for the eye and less affected by atmospheric attenuation. The pseudo-random bit sequence (PRBS) source is used to generate codes corresponding to the information signal in a binary format, followed by a non-return to zero (NRZ) pulse generator to convert the binary format signal to electrical signal. The Mach-Zehnder modulator (MZM) does the modulation for the laser beam with respect to the electrical output produced by the NRZ pulse generator, and next, the modulated signal is transmitted through the propagation free-space channel [14, 15]. At the receiver part, a PIN photodetector converts the optical signal into an electrical signal, and any high-frequency noise present in the signal can be filtered by a low-pass Bessel filter and sent for inspection by an eye diagram analyser to see the quality of the eye diagram, minimum bit-error rate (BER) and Q-factor of the designated system. The signal power consumption while transmitted toward the receiver was also studied using optical power meters and the values of the link parameters shown in Table 2.

Table 2.

Simulation parameters.

Design parameter	Values
Operating wavelength, λ	1550 nm
Link distance, L	$1 \leq L \leq 7$ km
Diameter of the transmitter aperture	5 cm
Aperture diameter of the receiver	20 cm
Optical signal power	20 dBm
Beam divergence	2 mrad
Cut-off frequency	7.5 GHz
Type of the receiver	PIN
Bit rate	1.25 GBits/s
Modulation type	NRZ

3.3. Attenuation due to scintillation

To find the attenuation due to scintillation for any region such as Sulaimani City in this work, the authors had first to find the value of the total C_n^2 . This was performed by using the previous equations (1)–(4) from the parameters of Table 1 which were averaged over 10 years and tabulated in Table 3.

Table 3.

Monthly average C_n^2 values over 10 years from 2013 to 2022.

Month	C_n^2 ($\text{m}^{-3/2}$) $\cdot 10^{-14}$
January	3.146
February	3.441
March	3.966
April	4.728
May	5.566
June	7.075
July	8.197
August	7.870
September	6.795
October	5.287
November	4.245
December	3.565

Using the aforementioned equation (5) that relates the scintillation index (σ_I^2) to the C_n^2 , the monthly average values for the scintillation index for 120 months from 2013 to 2022 and for communication links (1–7 km) have been calculated in dB² units and listed in Table 4.

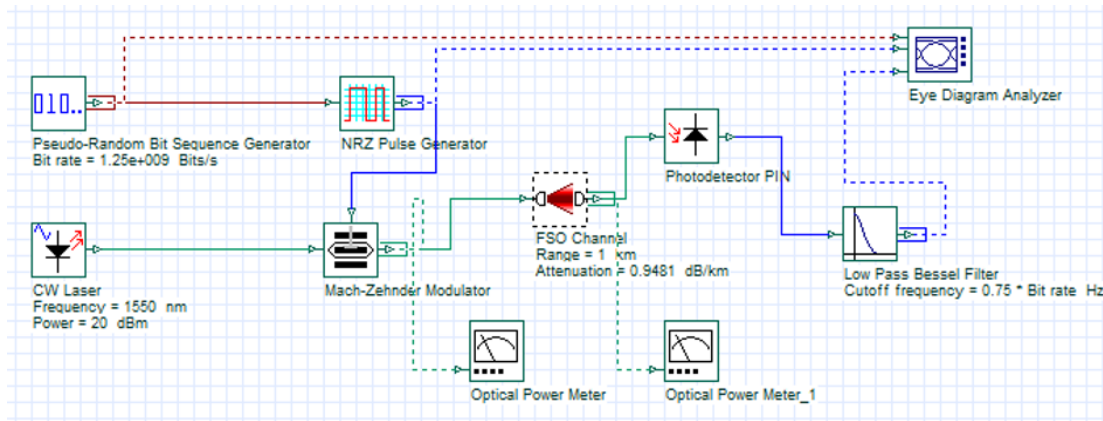


Fig. 1. Block diagram of the FSO link simulation model.

Table 4.
Scintillation index (σ_I^2) in dB², values for the average of 120 months from 2013 to 2022 per distance from 1 to 7 km.

Month	1 km	2 km	3 km	4 km	5 km	6 km	7 km
January	0.2247	0.7988	1.6777	2.4018	4.2726	5.9648	7.9087
February	0.2458	0.8762	1.8350	3.1065	4.6732	6.5241	8.6503
March	0.2832	1.0071	2.1149	3.5725	5.3862	7.5194	9.9701
April	0.3377	1.2005	2.5214	4.2684	6.4211	8.9642	11.8857
May	0.3975	1.4133	2.9682	5.0250	7.5592	10.5131	13.9924
June	0.5052	1.7965	3.7728	6.3873	9.6086	13.4141	17.7859
July	0.5854	2.0814	4.3713	7.4002	11.1324	15.5420	20.6065
August	0.5620	1.9983	4.1967	7.1047	10.6878	14.9208	19.7836
September	0.4853	1.7254	3.6235	6.1343	9.2280	12.8828	17.0813
October	0.3776	1.3425	2.8195	4.7732	7.1805	10.0246	13.2914
November	0.3032	1.0779	2.2637	3.8329	5.7652	8.0484	10.6712
December	0.2546	0.9053	1.9012	3.1285	4.8417	6.7593	8.9622

From the above Table 4 and using (6) attenuation $\alpha_{scint} = 2\sigma_I$ due to scintillation α_{scint} in dB are calculated and tabulated in Table 5.

Usually, in communication science, attenuation is measured in dB/km, so from the Table 5, the average atten-

uation values per link distance in dB/km for 120 months from 2013 to 2022 and distances from 1–7 km have been calculated as shown in Table 6 and used in the Optisystem-7 to analyse the performance of the proposed FSO communication link (Fig. 1).

Table 5.
Monthly average values of scintillation attenuation (α_{scint}) in dB over 10 years from 2013 to 2022 for link distances of 1–7 km.

Month	1 km	2 km	3 km	4 km	5 km	6 km	7 km
January	0.9481	1.7875	2.5910	3.0995	4.1341	4.8846	5.6245
February	0.9916	1.8721	2.7092	3.5251	4.2335	5.1085	5.8823
March	1.0643	2.0071	2.9085	3.7802	4.6416	5.4843	6.3151
April	1.1622	2.1913	3.1758	4.1320	5.0680	5.9881	6.8951
May	1.2610	2.3776	3.4457	4.4833	5.4988	6.4971	7.4813
June	1.4215	2.6807	3.8847	5.0546	6.1995	7.3251	8.4347
July	1.5302	2.8645	4.1815	5.4407	6.6731	7.8847	9.0789
August	1.4993	2.8272	4.0972	5.3310	6.5384	7.7156	8.8958
September	1.3933	2.6271	3.8071	4.9535	6.0755	7.1785	8.2659
October	1.2290	2.3173	3.3583	4.3695	5.3593	6.3323	7.2915
November	1.1013	2.0764	3.0091	3.9153	4.8022	5.6739	6.5334
December	1.0092	1.9030	2.7577	3.5375	4.4008	5.1997	5.9874

Table 6.
Scintillation attenuation (α_{scint}) in dB/km, monthly averaged for 10 years from 2013 to 2022 per distance from 1 to 7 km.

Month	1 km	2 km	3 km	4 km	5 km	6 km	7 km
January	0.9481	0.8938	0.8636	0.7749	0.8268	0.8141	0.8035
February	0.9916	0.9361	0.9031	0.8813	0.8467	0.8514	0.8403
March	1.0643	1.0036	0.9695	0.9451	0.9283	0.9141	0.9022
April	1.1622	1.0957	1.0586	1.0330	1.0136	0.9980	0.9850
May	1.2610	1.1888	1.1486	1.1208	1.0998	1.0829	1.0688
June	1.4215	1.3423	1.2949	1.2637	1.2399	1.2209	1.2050
July	1.5302	1.4323	1.3938	1.3602	1.3346	1.3141	1.2970
August	1.4993	1.4136	1.3657	1.3328	1.3077	1.2859	1.2708
September	1.3933	1.3136	1.2690	1.2384	1.2151	1.1964	1.1808
October	1.2290	1.1586	1.1194	1.0924	1.0719	1.0554	1.0416
November	1.1013	1.0382	1.0030	0.9788	0.9604	0.9457	0.9333
December	1.0092	0.9515	0.9192	0.8844	0.8802	0.8666	0.8553

4. Simulation analysis

The simulation of the FSO link (Fig. 1) was attained using the simulation parameters of Table 2, under different ranges from 1 to 7 km with their corresponding attenuations in dB/km in Table 6. The BER, that is the number of error bits while receiving the signal depending on the average received power, the scintillation strength, and the receiver noise [16] is presented in Table 8 taking under consideration the Q-factor recorded from the eye diagram analyser presented in Table 7.

The SNR can also be used to assess the quality of communication systems. For weak turbulence, the SNR is expressed as follows [9, 16]:

$$SNR = \frac{1}{(0.31 C_n^2 k^{7/6} L^{11/6})} \tag{7}$$

From (5)–(7), it can be easily calculated that:

$$SNR = \frac{1.613}{\sigma_1^2} = \frac{6.4516}{\alpha_{scint}^2} \tag{8}$$

In the above equation, α_{scint} values are given in dB, not dB/km. Thus, from Table 5, the monthly averaged SNR was calculated for 10 years from 2013 to 2022, per distance from 1–7 km, as shown in Table 9 below.

For a better performance analysis of the FSO communication, the optical power before and after the propagation channel, i.e., the free space, was also observed using an optical power meter and tabulated in Table 10.

Table 7 presents the Q-factor for the link, and it is clear that at a 6 km link distance, and for the months from June to September it starts decreasing to less than the acceptance value, which is 6 [17, 18]. Also, from the values of the BER in Table 8, it is clear that for the same months (June to September) and the same distance (6 km), the BER is more than 10^9 (which is the standard value of BER allowing only one error bit for 10^9 bits). From Tables 9 and 10, it is clear that the SNR and the output power decrease with the communication link length, respectively, for each month, with lower values in July and the highest values in January for any link distance. Figure 2 below shows the variation of the SNR during the months of the year for the link distance of 1–7 km.

Table 7.
The calculated maximum Q-factor.

Month	1 km	2 km	3 km	4 km	5 km	6 km	7 km
January	707	168.8	64.3	32.6	29.7	9.9	6.1
February	700.8	165.7	62.5	29.7	16.6	9.46	5.8
March	690.8	160.8	59.7	28.2	15.1	8.7	5.2
April	677.4	154.4	56.2	26.1	13.7	7.7	4.4
May	664.2	148	52.9	24.1	12.4	6.8	3.9
June	643.2	138.3	47.8	21.3	10.6	5.6	3.2
July	629.3	132.8	44.7	19.5	9.5	4.9	2.7
August	633.2	134	45.5	20.0	9.8	5.1	2.8
September	647	140.1	48.7	21.8	10.9	5.8	3.3
October	668.5	150.1	54.0	24.7	12.5	7.1	4.1
November	685.7	158.4	58.4	27.4	14.6	8.3	5.0
December	698.4	164.6	60.5	29.7	16.0	9.3	5.6

Table 8.
The calculated minimum BER.

Month	1 km	2 km	3 km	4 km	5 km	6 km	7 km
January	0.00	0.00	0.00	$3.3 \cdot 10^{-233}$	$7.3 \cdot 10^{-194}$	$1 \cdot 10^{-23}$	$4 \cdot 10^{-10}$
February	0.00	0.00	0.00	$7 \cdot 10^{-195}$	$4.1 \cdot 10^{-62}$	$1.5 \cdot 10^{-21}$	$3.6 \cdot 10^{-9}$
March	0.00	0.00	0.00	$8 \cdot 10^{-175}$	$5.8 \cdot 10^{-52}$	$2.1 \cdot 10^{-18}$	$8.7 \cdot 10^{-8}$
April	0.00	0.00	0.00	$2.4 \cdot 10^{-150}$	$3.7 \cdot 10^{-43}$	$6.2 \cdot 10^{-15}$	$2.6 \cdot 10^{-6}$
May	0.00	0.00	0.00	$3.5 \cdot 10^{-129}$	$8.5 \cdot 10^{-36}$	$3.8 \cdot 10^{-12}$	$8.5 \cdot 10^{-5}$
June	0.00	0.00	0.00	$9.2 \cdot 10^{-101}$	$1.8 \cdot 10^{-26}$	$8.6 \cdot 10^{-9}$	$8 \cdot 10^{-4}$
July	0.00	0.00	0.00	$3.9 \cdot 10^{-85}$	$1.2 \cdot 10^{-21}$	$3.8 \cdot 10^{-7}$	$3 \cdot 10^{-3}$
August	0.00	0.00	0.00	$2.6 \cdot 10^{-89}$	$6.4 \cdot 10^{-23}$	$1.4 \cdot 10^{-7}$	$2 \cdot 10^{-3}$
September	0.00	0.00	0.00	$2.6 \cdot 10^{-105}$	$6.3 \cdot 10^{-28}$	$2.7 \cdot 10^{-9}$	$5 \cdot 10^{-4}$
October	0.00	0.00	0.00	$1.1 \cdot 10^{-135}$	$2 \cdot 10^{-36}$	$5.5 \cdot 10^{-13}$	$1.7 \cdot 10^{-5}$
November	0.00	0.00	0.00	$5.1 \cdot 10^{-165}$	$1.9 \cdot 10^{-48}$	$5.3 \cdot 10^{-17}$	$3.5 \cdot 10^{-7}$
December	0.00	0.00	0.00	$7.3 \cdot 10^{-194}$	$9.9 \cdot 10^{-58}$	$9.9 \cdot 10^{-58}$	$8.3 \cdot 10^{-9}$

Table 9.
SNR monthly averaged for 10 years from 2013 to 2022 per distance from 1 to 7 km.

Month	1 km	2 km	3 km	4 km	5 km	6 km	7 km
January	7.1773	2.0192	0.9610	0.6716	0.3775	0.2704	0.2039
February	6.5614	1.8408	0.8790	0.5192	0.3600	0.2472	0.1865
March	5.6956	1.6015	0.7627	0.4515	0.2995	0.2145	0.1618
April	4.7765	1.3436	0.6397	0.3779	0.2512	0.1799	0.1357
May	4.0573	1.1413	0.5334	0.3210	0.2137	0.1528	0.1153
June	3.1928	0.8978	0.4275	0.2525	0.1679	0.1202	0.0907
July	2.7553	0.7863	0.3690	0.2180	0.1449	0.1038	0.0783
August	2.8701	0.8072	0.3843	0.2270	0.1509	0.1084	0.0815
September	3.3234	0.9348	0.4451	0.2629	0.1748	0.1252	0.0944
October	4.2713	1.2014	0.5720	0.3379	0.2246	0.1609	0.1213
November	5.3193	1.4964	0.7125	0.4209	0.2798	0.2004	0.1511
December	6.3345	1.7815	0.8483	0.5156	0.3331	0.2386	0.1800

Table 10.
The output power of the system before the PIN photo diode.

Month	1 km (μW)	2 km (μW)	3 km (μW)	4 km (μW)	5 km (μW)	6 km (μW)	7 km (μW)
January	376.6	79.5	29.6	14.9	13.1	4.4	2.7
February	372.9	78	28.8	13.5	7.35	4.18	2.57
March	366.7	75.6	27.5	12.7	6.7	3.8	2.33
April	358.5	72.5	25.9	11.7	6.1	3.4	2
May	350.4	69.4	24.3	10.8	5.5	3	1.7
June	338	64.7	22	9.5	4.67	2.5	1.4
July	329.4	62.1	20.5	8.7	4.2	2.2	1.2
August	332	63	21	8.9	4.32	2.3	1.3
September	340	65.5	22.4	9.7	4.8	2.6	1.48
October	353	70.4	24.8	11.1	5.5	3.2	1.86
November	363.5	74.4	27	12.33	6.5	3.7	2.2
December	371.3	77.4	28	13.5	7.1	4.1	2.5

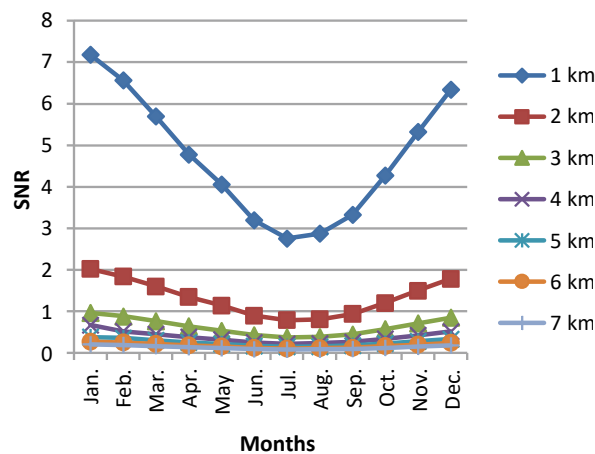


Fig. 2. Variation of SNR month to month different link distances.

The data from Tables 8 and 9 indicate that the BER and the SNR for any FSO communication link vary inversely with each other, indicating that the system is efficient. From the values of the Q-factor and BER (Tables 7 and 8) of the system, it is clear that the satisfactory link distance for the case study is between 5 and 6 km, so to get the

optimal link distance for the feasibility of FSO, the same previous procedure has been repeated to find the optimal link distance, which was 5.5 km. The calculation for the scintillation attenuation at 5.5 km corresponding to all the average months has been found, and the simulation outputs are tabulated in Table 11.

Table 11.
Monthly averaged 10 years (from 2013 to 2022) attenuation, SNR, maximum Q-factor, BER, and output power for a 5.5 km link distance.

Month	Attenuation (dB/5.5 km)	SNR	Max. Q-factor	BER	Output power (μW)
January	0.8201	0.3171	12.9119	$1.92 \cdot 10^{-38}$	5.707
February	0.8577	0.2899	12.3146	$3.76 \cdot 10^{-35}$	5.442
March	0.9208	0.2515	11.371	$2.91 \cdot 10^{-30}$	5.024
April	1.0054	0.2109	10.2143	$8.52 \cdot 10^{-25}$	4.513
May	1.0909	0.1792	09.1609	$2.56 \cdot 10^{-20}$	4.050
June	1.2299	0.1410	07.6689	$8.65 \cdot 10^{-15}$	3.397
July	1.3238	0.1217	06.7973	$5.31 \cdot 10^{-12}$	3.016
August	1.2972	0.1268	07.0339	$1.00 \cdot 10^{-12}$	3.119
September	1.2053	0.1468	07.9146	$1.24 \cdot 10^{-15}$	3.504
October	1.0632	0.1887	09.4902	$1.15 \cdot 10^{-21}$	4.195
November	0.9527	0.2350	10.9208	$4.57 \cdot 10^{-28}$	4.825
December	0.8730	0.3872	12.0791	$6.78 \cdot 10^{-34}$	5.336

From the data in Table 11, for the case studied, the variation of the maximum Q-factor and the output power of the signal while propagating through the free space with the months have been evaluated as shown in Figs. 3 and 4, respectively.

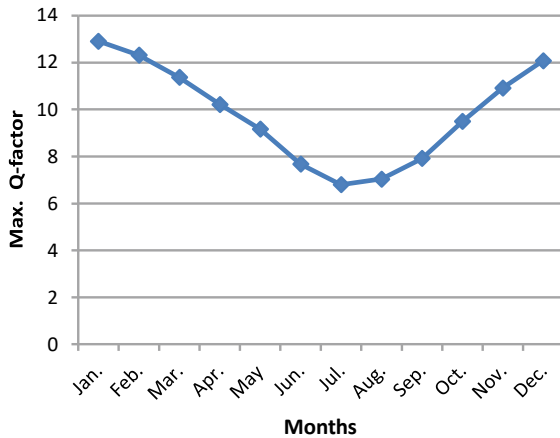


Fig. 3. Q-factor vs. months for a 5.5 km link distance.

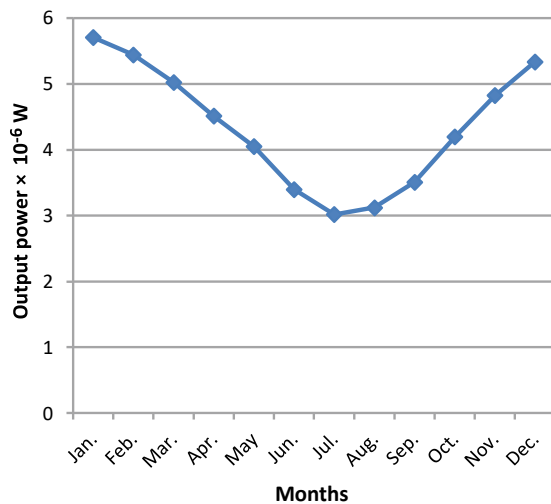


Fig. 4. Output power vs. months for a 5.5 km link distance.

The eye diagram that indicates the quality and performance of the communication presented in Fig. 5 shows the variation of the communication level with the months of the year through the eye opening.

5. Results analysis

From Table 6, which presents the values of the attenuation due to scintillation in dB/km, it is quite obvious how this attenuation varies with the months because of their variation in meteorological parameters such as relative humidity, temperature, and wind speed. Scintillation attenuation α_{scint} values are also inversely proportional to the link distance for all the months. Figure 6 shows these variations.

For Sulaimani City and for any link distance, the minimum scintillation attenuation in dB/km was recorded in January and the maximum attenuation was in July (see Table 6). This corresponds to the C_n^2 values variation with the months. Figure 7 shows the variation of the average C_n^2 for 120 months of the years 2013–2022.

Ten-year (2013–2022) monthly average changes in relative humidity, temperature, and wind speed by months contributed to the calculation of the C_n^2 for the case studied which is summarised in Fig. 8 below.

The availability and feasibility of FSO communication for Sulaimani City (study case) can be further estimated using the Q-factor values from Table 7. The maximum values appear in January and the minimum are in July, decreasing with increasing link distances from 1 to 7 km. There are some months between 5 and 6 km (June to September) when the Q-factor values are lower than the accepted value (6). The same thing can be achieved and observed from the BER values of the communication, which can tell how much error has occurred in the bit sequence while the signals were transferred from the transmitter to the receiver. For optimal communication, the BER is 10^{-9} and below. From Table 8, it is clear that up to a distance of 3 km and for all months, there are no errors in the bit sequence while propagating toward the receiver. The errors start being detected at 4 km and increase as the

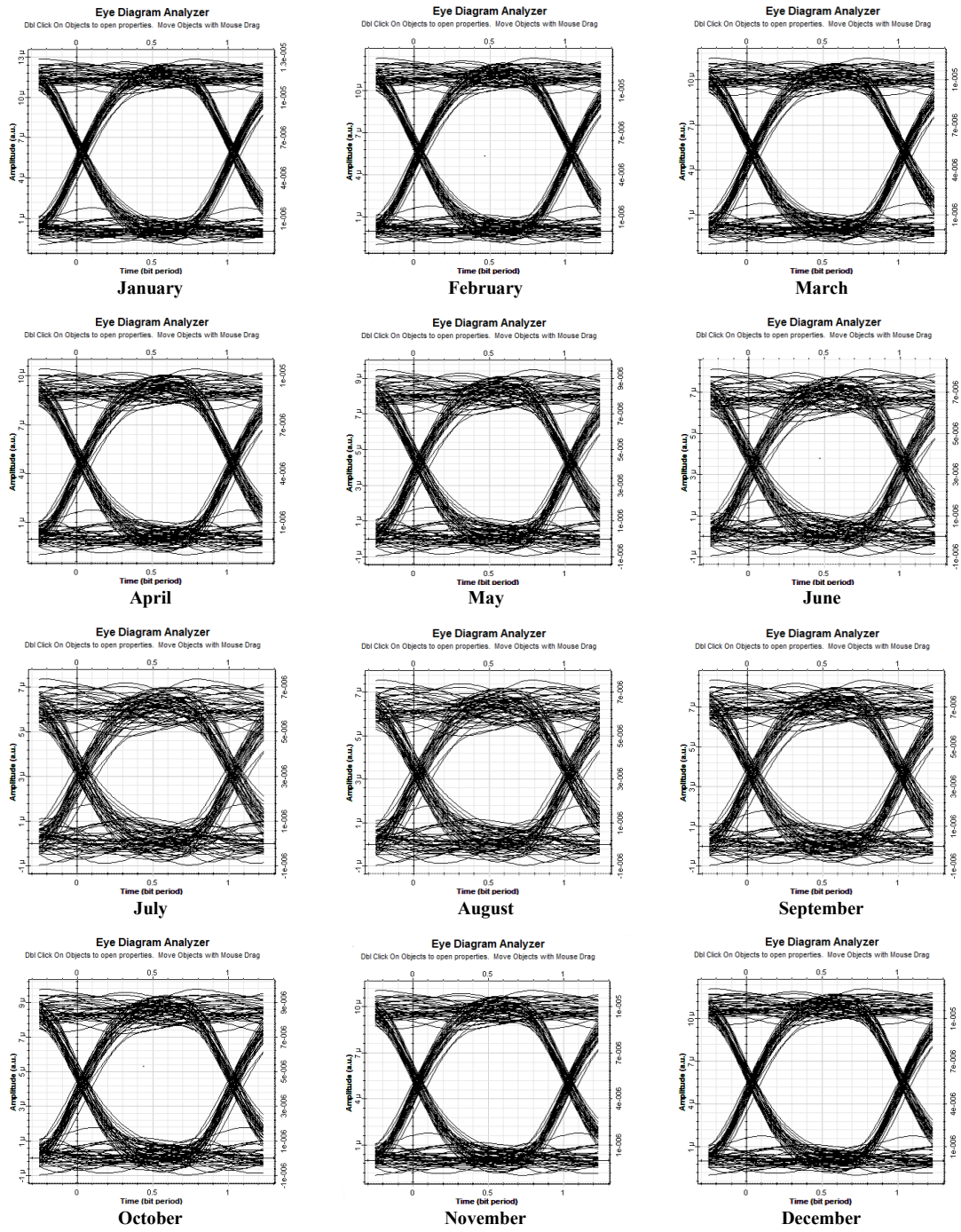


Fig. 5. Eye diagram for the monthly average five years under 5.5 km link distance.

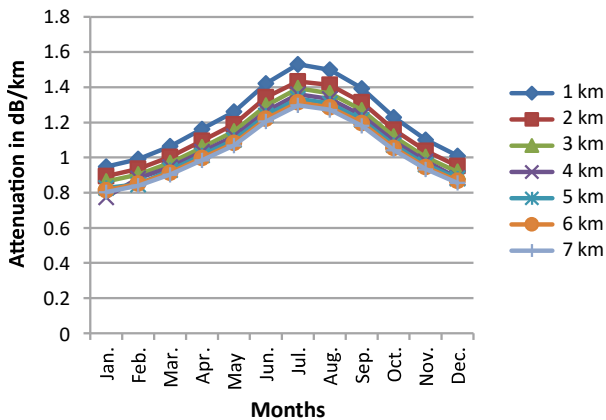


Fig. 6. Attenuation vs. months for different link distance.

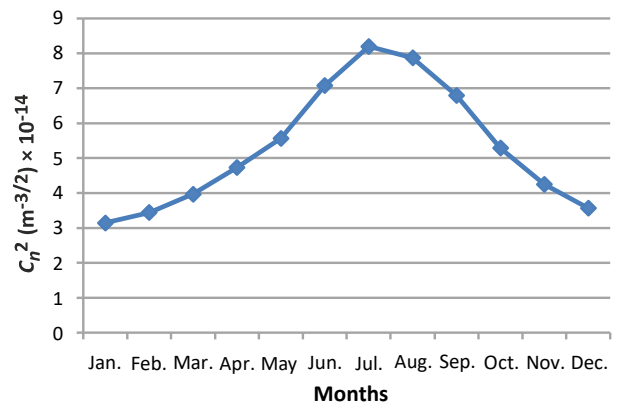


Fig. 7. Variation of the monthly average C_n^2 for the years from 2013 to 2022.

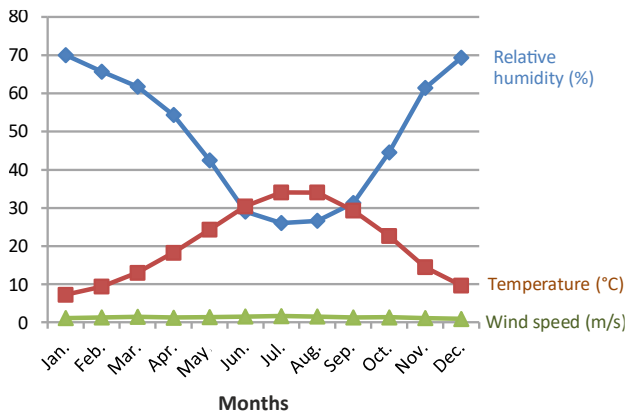


Fig. 8. Monthly average relative humidity, temperature, and wind speed variations from month to month from 2013 to 2022.

distance increases for all months. The minimum errors observed were in January and the maximum in July. In general, all the values are accepted until 5 km, after that, the quality of the communication degrades and is not allowed for the months from June to September with BER values higher than 10^{-9} . Table 10, containing the output power of the signal after reaching the receiver, emphasises the effect of different months having different scintillation attenuation for different link distances on the quality of the FSO communication performance. In January, the signal reaches the receiver with higher power than in July for all distances.

All the above observations led to thinking about the optimal link distance for the FSO communication in Sulaimani City as the study case and after simulation it has been found that the optimal link in Sulaimani City is 5.5 km, at which all the analyser parameters have their accepted values as their monthly average values for the years 2013–2022 tabulated in Table 11. The Q-factor and the output power variations with the months shown in Figs. 3 and 4, respectively, show how these parameter values decrease from January to September and start increasing again.

The eye diagrams presented in Fig. 5, describing the performance quality of the communication system at 5.5 km, show how the eye opening varies by month indicating that for this case (Sulaimani City) the high quality communication will be in winter (January) and the low quality will be in summer, especially in July.

6. Conclusions

The monthly average C_n^2 for 10 years has been calculated for the studied area as tabulated in Table 4, and all the values are more than 10^{-14} so the scintillation level is in the strong regime. This is the essential parameter for calculating the scintillation attenuation needed before installing FSO communication in any place.

The same fact can be concluded from the values of σ_1^2 from Table 5. All the values are higher than one $\sigma_1^2 > 1$ except for 1 km link distance [8, 10, 12]. As σ_1^2 increases with the link distance, the attenuation in dB also increases, but its value in dB/km decreases very slightly. The variations of σ_1^2 and α_{scint} in dB/km from month to month are similar.

The variation of σ_1^2 and the BER as a function of link distance and months are similar. The variation of σ_1^2 and each of the Q-factors, SNR and the output power as a function of link distance and months are exactly opposite.

The FSO system availability decreases with increasing propagation link, and an approximate link distance can be calculated to be 5.5 km for the study area. The eye-opening description of the quality of the communication varies from month to month. The best and worst seasons of FSO communication for any country can be found before installing and performing this technology.

Acknowledgements

Meteorology Station of Sulaimani City for supporting this work through supplying all the data for 10 years from 2013 to 2022.

References

- [1] Rashidi, F. & Semakuwa, S. Analysis of rain effect in free space optical communication under nrz modulation in two regions of Tanzania. *Int. J. Adv. Eng. Nanotechnol.* **1**, 13–16 (2014). <https://www.ijaent.org/wp-content/uploads/papers/v1i10/J02150911014.pdf>
- [2] Alkholidi, A. & Altowij, K. Effect of Clear Atmospheric Turbulence on Quality of Free Space Optical Communications in Western Asia. in *Optical Communications Systems* (ed. Das, N.) 41–74 (IntechOpen, 2012). <https://doi.org/10.5772/35186>
- [3] Sony, K., Kurella, S., Mallisetty, R., San Vardhan, B. & Datta, M. S. S. Analysis of FSO system under clear and rain conditions. *Int. J. Recent Technol. Eng.* **7**, 924–928 (2019). <https://www.ijrte.org/wp-content/uploads/papers/v7i6/F2546037619.pdf>
- [4] Al Naboulsi, M., Sizun H. & de Fornel, F. Propagation of optical and IR waves in the atmosphere. *Environ. Sci.* **7**, 01729 (2005). [https://www.ursi.org/proceedings/procGA05/pdf/F01P.7\(01729\).pdf](https://www.ursi.org/proceedings/procGA05/pdf/F01P.7(01729).pdf)
- [5] Twati, M., Badi, M. & Adam, F. Analysis of rain effects on free space optics based on data measured in the Libyan climate. *Int. J. Inf. Electron. Eng.* **4**, 469–472 (2014). <https://doi.org/10.7763/IJIEE.2014.V4.485>
- [6] Vitásek, J. *et al.* Atmospheric Turbulences in Free Space Optics Channel. in *34th International Conference on Telecommunications and Signal Processing (TSP)* 104–107 (IEEE, 2011). <https://doi.org/10.1109/TSP.2011.6043763>
- [7] *Optical Communication Systems* (ed. Das, N.) (IntechOpen, 2012), <https://www.intechopen.com/books/1339>
- [8] Ali, M. A. A. Atmospheric turbulence effect on FSO communications. *Int. J. Emerg. Technol. Comput. Appl. Sci.* **5**, 345–351 (2013). <http://iasir.net/IJETCASpapers/IJETCAS13-364.pdf>
- [9] Motlagh, A., Ahmadi, V., Ghassemlooy, Z. & Abedi, K. The Effect of Atmospheric Turbulence on the Performance of the Free Space Optical Communications. in *Proceedings of the 6th International Symposium on Communication Systems, Networks and Digital Signal Processing* 540–543 (IEEE, 2008). <https://doi.org/10.1109/CSNDSP.2008.4610725>
- [10] Tunick, A. Optical turbulence parameters characterized via optical measurements over a 2.33 km free-space laser path. *Opt. Express* **16**, 14645–14654 (2008). <https://doi.org/10.1364/OE.16.014645>
- [11] Sadot, D. & Kopeika, N. Forecasting optical turbulence strength on the basis of macroscale meteorology and aerosols: models and validation. *Proc. SPIE* **31**, 200–212 (1992). <https://doi.org/10.1117/12.56059>
- [12] Demir, P. & Yilmaz, G. The investigation of SNR for Free Space Optical Communication Under Turbulence. *Karalimas Sci. Eng. J.* **8**, 438–445 (2018). <https://dergipark.org.tr/tr/download/article-file/1329012>
- [13] Canuet, L. Atmospheric turbulence profile modeling for satellite-ground laser communication. (Universitat Politècnica de Catalunya, 2014).

- [14] Krishnan, P. Performance Analysis of FSO Systems over Atmospheric Turbulence Channel for Indian Weather Conditions. in *Turbulence and related phenomena* (ed. Barillé, R.) ch 2 (IntechOpen, 2019). <https://doi.org/10.5772/intechopen.80275>
- [15] Grover, M. Singh, P. & Kaur, P. Mitigation of scintillation effects in WDM FSO system using multibeam technique. *J. Telecommun. Inf. Technol.* **2**, 69–74 (2017). <https://jtit.pl/jtit/article/view/666/666>
- [16] Altowij, K. S., Alkholidi, A. & Hammam, H. Effect of clear atmospheric turbulence on quality of free space optical communications in Yemen. *Front. Optoelectron. China* **3**, 423–428. 2010. <https://doi.org/10.1007/s12200-010-0123-8>
- [17] Maurya, V. Design and Performance Analysis of VLC System with Noise Mitigation. *Malaviya National Institute of Technology Jaipur* <http://idr.mnit.ac.in/handle/123456789/554> (2019).
- [18] El-Mokadem, E., Tawfik, N., Aly, M. & El-Deeb, W. Design and performance evaluation of vehicular visible light communication system under different weather conditions and system parameters. *Opto-Electron. Rev.* **31**, e145580 (2023). <https://doi.org/10.24425/opelre.2023.145580>